The Role of Copper on the Crevice Corrosion Behavior of Nickel-Chromium-Molybdenum Alloys in Aggressive Solutions

A.K. Mishra,[*,**] X. Zhang,[*,***] and D.W. Shoesmith[‡,*,****]

ABSTRACT

The effect of Cu on the localized corrosion of Ni-Cr-Mo alloys has been investigated in hot saline solutions by comparing the behavior of N06059 and N06200 alloys, using electrochemical and surface analytical techniques. No measurable effect of copper on anodic film growth kinetics and passive film properties was detected and the breakdown and repassivation potentials of the alloys were very similar. Angle-resolved x-ray photoelectron spectroscopy and time-of-flight secondary ion mass spectroscopy demonstrated that the copper segregated to the oxide/solution interface during anodic film growth and that this process was enhanced as the pH decreased, as would occur in a crevice prior to initiation. Galvanostatically controlled crevice corrosion experiments demonstrated that this surface accumulation suppressed the metastable breakdown events that preceded initiation on the Cu-free alloy. Dynamic secondary ion mass spectrometry showed that copper accumulated with molybdates in crevice corroded locations but could not confirm any influence of copper on crevice propagation.

KEY WORDS: copper, crevice corrosion, dynamic-secondary ion mass spectroscopy, energy-dispersive x-ray spectroscopy, Ni-Cr-Mo alloys, potentiodynamic-galvanostatic-potentiodynamic technique, scanning electron microscopy, time-of-flight secondary ion mass spectroscopy, x-ray photoelectron spectroscopy

INTRODUCTION

Nickel-based alloys are widely used in aggressive environments because of their good corrosion resistance. With the addition of the optimum amounts of chromium and molybdenum, the corrosion resistance increases significantly in both reducing and oxidizing environments,[1-7] although they may be susceptible to crevice corrosion under aggressive conditions.[8-15] One approach to improve the localized corrosion resistance of these alloys is to add small amounts of Cu. The effect of Cu addition on corrosion resistance, particularly localized corrosion, has been studied in detail for stainless steel (SS)[16-28] and to a lesser extent aluminum alloys.[29-31] However, to date, no focused study of the effect of Cu on the localized corrosion of Ni-Cr-Mo alloys has been published and the question remains as to whether its addition provides any value.

The beneficial effect of adding Cu to SS has been widely reported, but some researchers have demonstrated detrimental effects. Sourisseau, et al.,[16] studied the effect of 0.2 wt% and 3.0 wt% Cu addition on the pitting of austenitic SS in chloride solution. The addition of 3.0% Cu decreased the pitting and repassivation potentials and increased the charge associated with metastable pits as deduced from current transient analysis, suggesting that Cu addition delayed repassivation and promoted pit stabilization. By contrast, Cu addition also lowered the anodic

Submitted for publication: August 10, 2015. Revised and accepted: October 21, 2015. Preprint available online: October 26, 2015, http://dx.doi.org/10.5006/1876.
‡Corresponding author. E-mail: dwshoesm@uwo.ca.
*Department of Chemistry, Western University, London, ON, N6A 5B7, Canada.
**Research & Technology, Haynes Int., Kokomo, IN 46901.
***McMaster University, Hamilton, ON, Canada.
****Surface Science Western, 999 Collip Circle, London, ON, N6G 0J3, Canada.

ISSN 0010-9312 (print), 1938-159X (online)
16/000051/$5.00+$0.50/0

dissolution rates and pit propagation rates in acidic chloride solution. It was claimed that x-ray photoelectron spectroscopy (XPS) (results not shown in the article) demonstrated an enrichment of metallic Cu on active sites, which inhibited repassivation by preventing oxidation of the underlying Fe or Cr. However, this surface enrichment had a counterbalancing beneficial effect by forming a barrier layer to base metal dissolution.

Lin, et al.,[17] investigated the effect of Cu additions on the corrosion of austenitic SS in 0.1 M H_2SO_4 solution. The difference between the pit nucleation and protection potentials decreased with an increase in Cu content (0.4% to 3.0%), indicating an enhanced resistance to localized corrosion. The properties of the oxide films grown at applied potentials of 400 mV_{SCE} and –400 mV_{SCE} were characterized by XPS and Auger electron spectroscopy (AES). While an enrichment of Cu was observed at the lower potential, no Cu peak was observed at 400 mV. The Pourbaix diagram[32] indicates that Cu should dissolve as Cu(II) in acidic solution at 400 mV, but be stable as either Cu_2O or metallic Cu at –400 mV. Unfortunately, the XPS peaks for Cu_2O and metallic Cu were very close,[33] making it difficult to distinguish them by XPS.

Jiangnan, et al.,[18] showed that Cu decreased the anodic dissolution rate of austenitic SS (18Cr-10Ni-2Cu) in 3.5% NaCl solution at 80°C, and surface characterization techniques indicated this could be attributed to enrichment of Cu on the surface. No influence of Cu surface enrichment or of Cu(II) dissolved in solution on passive film behavior was observed. However, the passivation kinetics of the SS containing Cu were slower than those of the Cu-free alloy.

Seo, et al.,[19] and Hultquist, et al.,[20] studied the corrosion resistance of Cu-containing ferritic SS in sulfuric acid and neutral sodium chloride solutions. Polarization curves showed active dissolution was suppressed on the 0.4 wt% Cu-containing ferritic SS, and AES studies indicated this could be attributed to the surface enrichment of Cu at active potentials. In the passive and transpassive regions, no Cu enrichment was detected. Additionally, potential decay curves measured in a 1 M H_2SO_4 + 0.5 M NaCl solution yielded a slower reactivation time (time required for reactivation as a result of breakdown of the passive film) on specimens containing Cu. These results suggest a detrimental effect of Cu on passive film stability and it was concluded that at high potentials, metallic Cu dissolves as Cu(II) to form active sites and a less stable passive film.

Itzhak and Peled[21] showed that a small amount of Cu (0.25 wt%) in sintered 316SS (UNS S31600)[(1)] increased the corrosion potential by ~450 mV and decreased the passivation and critical current densities by two orders of magnitude. These effects were attributed to the selective anodic dissolution of the active surface leading to local enrichment of noble Cu, as confirmed by AES.[22] Ujiro, et al.,[25] reported a beneficial effect of Cu on the pitting of austenitic and ferritic SS in chloride media in an active potential range but a harmful effect when pitting occurred at more noble potentials. Improvements in localized corrosion behavior have also been reported for duplex SS (DSS)[26] and 204Cu SS (UNS S20430),[27] and it was suggested that enrichment of metallic Cu within a pit resulted in a lower anodic dissolution current.

TABLE 1

Nominal Alloy Compositions (wt% of major alloying element)

Major Alloying Element	N06059	N06200
Cr	23	23
Mo	16	16
Cu	-	1.6
Ni	bal.	bal.

While most research on the influence of Cu alloying has been focused on SS, recent studies reported the inhibition of localized corrosion on Al alloys resulting from Cu alloying.[30-31] The presence of Cu in solid solution in an Al matrix increases the pitting potential in chloride solution, but this improvement is limited by the solubility of Cu in Al.[29] Kim and Buchheit[30] demonstrated an inhibiting effect of Cu on metastable pitting in chloride solution: Cu in the solid solution retarding stable pit formation by inhibiting the initiation of metastable pits. Also, suppression of peak pitting currents inhibited metastable pit growth. This lowers the probability of stable pit formation resulting in an increase in pitting potential. Further, scanning transmission electron microscopy images showed localized Cu enrichment in the base of the pit.[31]

Some studies on the role of Cu in Ni-Cr-Mo alloys have been reported. Sridhar[34] claimed a beneficial role for Cu addition in Ni-22Cr-6Mo-25Fe in various concentrations of sulfuric acid. The addition of even a small amount of Cu (~2 wt%) significantly reduced the corrosion rate in high concentrations of sulfuric acid. Crook, an inventor of the Cu-containing C-2000[†] (UNS N06200) alloy,[35-36] investigated the corrosion performance of this alloy in a wide range of corrosive media and clearly demonstrated a higher uniform corrosion resistance of N06200 compared to other corrosion resistant Ni-Cr-Mo alloys. VanGansbeke, et al.,[37] appeared to confirm the results of Sridhar[34] in a comparison of these two alloys in various aggressive solutions. A similar noticeable difference in corrosion performance of these two alloys was observed in high concentrations of sulfuric acid.[34] Because the only compositional difference is the presence of Cu in N06200 (Table 1), its addition appeared to be beneficial.

[(1)] UNS numbers are listed in *Metals and Alloys in the Unified Numbering System*, published by the Society of Automotive Engineers (SAE International) and cosponsored by ASTM International.

[†] Trade name.

Recently, Zhang, et al.,[38-39] studied the passive film behavior of the N06200 alloy in chloride solutions. Using angle-resolved x-ray photoelectron spectroscopy (AR-XPS) and time-of-flight secondary ion mass spectroscopy (TOF-SIMS), it was shown that the outermost layer of the passive film was enriched with Cu (or Cu[I] oxide) and Mo, the intermediate region was dominated by Cr/Ni hydroxides, and the inner region was composed of the expected Cr(III) oxide barrier layer. It was not clear if the presence of Cu in the outer regions of the oxide had any influence on passivity. Despite these studies, there is little to no literature available on the effect of Cu alloying on the localized corrosion behavior of Ni-Cr-Mo alloys.

In this study, the effect of Cu on the localized corrosion of the N06200 alloy has been investigated in hot saline solutions by comparing its behavior to that of the Alloy 59† (UNS N06059) alloy, which has a similar composition except for the absence of Cu. Crevice corrosion experiments were conducted using either a multiple crevice assembly (MCA)[8-13] to determine breakdown (E_b) and repassivation ($E_{R,CREV}$) potentials or a single crevice arrangement[14] in 1 M NaCl to follow the crevice initiation process. On completion of electrochemical experiments, the corroded regions were characterized using optical microscopy, scanning electron microscopy (SEM), energy-dispersive x-ray spectroscopy (EDX), and dynamic-secondary ion mass spectroscopy (dynamic-SIMS).

EXPERIMENTAL PROCEDURES

Materials and Electrode Preparation

Electrodes were cut from plates of the N06200 and N06059 alloys. The nominal alloy compositions are given in Table 1. The electrodes were drilled at one end to allow electrical connection to a threaded rod of the same material. The rod was sheathed in glass and sealed with a Teflon† (PTFE) gasket to prevent contact with electrolyte when in the electrochemical cell. These electrodes were polished with a series of wet SiC papers up to 1200 grit. The electrodes used in experiments designed to study passive films were further polished successively with a 5.0, 0.3, and 0.5 μm alumina powder suspensions. The electrodes were then rinsed with deionized water and acetone and dried. On placement in the electrochemical cell, electrodes were only partially immersed in the solution to avoid the possibility of a crevice at the PTFE/specimen interface. In experiments to study passive film properties, the electrodes were immediately placed in the cell after polishing and rinsing.

Electrochemical Experiments and Solutions

Electrochemical experiments were conducted in a standard three-electrode jacketed cell connected to a water circulating bath (Isotemp 3016H†, Fisher Scientific) to maintain the temperature of the solution to within ±1°C. A Pt foil was used as the counter electrode and either a commercial saturated calomel electrode (SCE) (–0.242 V_{SHE} at 25°C) or an in-house fabricated silver/silver chloride (Ag/AgCl) electrode (–199 mV_{SHE} at 25°C) was used as the reference electrode. The reference and counter electrodes were housed in separate compartments attached to the main body of the cell through glass grits. Unless otherwise stated, experiments were conducted in freshly-prepared 1 M NaCl solutions prepared from reagent grade NaCl and ultrapure deionized water obtained from a Milli-Q Academic A-10† system. When required, the pH of the solutions was adjusted using HCl and NaOH solutions. Prior to each experiment, the electrolyte solution was purged for at least 1 h in ultra high purity Ar (Praxair†) and purging continued throughout the experiment.

In polarization and potentiostatic experiments, a Solartron 1284† multistat was used to apply potentials and CorrWare Software† (Scribner Associates) was used to record current data. In polarization experiments, the corrosion potential (E_{corr}) was recorded for 1 h before scanning the potential from 200 mV below E_{corr} to 200 mV_{SCE} at a scan rate of 0.167 mV/s. After potentiostatic film growth experiments, the electrode was immediately removed from the cell, rinsed and ultrasonicated for 2 min in pure deionized water to remove electrolyte, and dried in a stream of Ar gas before transfer to the vacuum chamber of the surface analytical equipment.

Multiple Crevice Assembly Experiments

The geometry of the working electrode was similar to that described earlier but with a 7.0 mm diameter hole machined in the center of the cubic specimen to allow assembly of the multiple crevice assembly (MCA). Prior to an electrochemical experiment, samples were polished with a series of wet SiC papers up to 1200 grit, rinsed with deionized water and acetone, and air dried. A PTFE-wrapped ceramic crevice former, tightened to a torque of 70 in·lbf (7.91 N·m) by Ti bolts, was used to create 12 crevices. A Pt foil and a SCE were used as the counter and reference electrodes, respectively.

Similar electrochemical cell and temperature controller arrangements to those described earlier were used. Crevice corrosion experiments were performed in the jacketed electrochemical cell using the potentiodynamic-galvanostatic-potentiodynamic (PD-GS-PD) technique[8] to measure the E_b and $E_{R,CREV}$. Potentiodynamic scans were performed at a scan rate of 0.167 mV/s from a potential 150 mV below E_{corr} to a potential above E_b until a current of 30 μA was reached. This current was then maintained galvanostatically for 35 h. Finally, the potential was scanned back to a lower potential at a rate of 0.167 mV/s. Galvanostatic control was maintained for 35 h,[9] rather than the normal 2 h.[8] In the present study, because many experiments were performed, not all of

the experiments reported were reproduced. However, a few experiments were selected randomly and repeated to ensure the results were reproducible.

Single Crevice Assembly Experiments

Single crevice assembly (SCA) experiments were conducted inside a pressure vessel, which allows boiling to be suppressed at T > 100°C. The vessel was lined with a 3 mm thick cylindrical PTFE liner to avoid direct solution contact with the wall of the Ti pressure vessel. The creviced (working) electrode was suspended from a thin cylindrical rod of the same material enclosed in heat-shrink PTFE tubing to avoid electrical contact with the pressure vessel. The counter electrode was made from the same material as the working electrode. A homemade Ag/AgCl (saturated KCl) reference electrode was used.[40] The potential of this electrode (–45 mV_{SCE}) was checked against a commercial SCE, used only as a standard, before and after each experiment.

A schematic of the crevice electrode arrangement inside the pressure vessel has been reported previously.[14] The geometry of the working electrode was designed to avoid unwanted crevices. The crevice former was a PTFE slice fixed between the flat metal surface and a polysulfone coupon. In this study the crevice design was modified slightly, with the crevice former surface area made smaller than the flat surface area of metal, in order to better define the crevice mouth and to confine any propagation to the flat surface of the specimen. The creviced assembly was held together with insulated threaded bolts and metal nuts to ensure that the defined working electrode surface would be the only creviced metal area exposed to solution. The creviced face of the working electrode was polished using the same procedure used with the MCA.

Experiments were performed in aerated 1 M NaCl and the temperature of the solution was 105°C. To prevent boiling of the electrolyte solution, the vessel was pressurized with 0.4 MPa of Ar gas. On first exposure to the solution, the electrode was allowed to stabilize at E_{corr} for 8 h. Subsequently, crevice corrosion was initiated galvanostatically (5 µA, 10 µA, and 20 µA) and the current maintained throughout the 48 h experiment.

Characterization Techniques

SEM images of the surfaces were obtained on a LEO 440† SEM equipped with an EDAX† EDX system at Surface Science Western. AR-XPS was performed on a Kratos Axis Ultra Spectrometer† using a monochromatic Al K_α (1,486.6 eV) source. The instrument work function was calibrated to give an Au $4f_{7/2}$ metallic Au binding energy of 83.95 eV. The spectrometer dispersion was adjusted to give a binding energy of 932.63 eV for the metallic $Cu2p_{3/2}$ peak. The Kratos charge neutralizer system was used for all analyses. The apparent shifts of the spectra were calibrated using the C1s peak set to 284.8 eV. High-resolution spectra were obtained using a 20 eV pass energy, whereas survey spectra were recorded using a 160 eV pass energy with an analysis area of ~300 µm × 700 µm. Two photoelectron take-off angles (measured from the sample surface), 30° and 90°, were used to analyze the oxide film. By comparison of the information obtained at a grazing take-off angle (30°C) to that obtained at an angle close to the surface normal (90°C), information on the variation of composition with depth was obtained.

An ION-TOF-SIMS was used to record TOF-SIMS depth profiles and cross-sectional images for sputtered specimens. A 1 kV Cs^+ ion beam was used to sputter an area of 200 µm × 200 µm on a specimen and negative secondary ions were collected from a 100 µm × 100 µm area within the sputter crater using a 25 kV monoisotopic Bi_3^+ primary ion beam. A smaller analysis area was used within the sputter crater to avoid edge effects. Each TOF-SIMS mass spectrum was calibrated using the exact mass values of at least three known species in the spectrum collected during profiling.

Elemental depth profiling was performed with a Cameca IMS-3f† ion microscope, using a 300 nA, 5.5 eV Cs^+ beam rastered over a 250 × 250 $µm^2$ area. Negative secondary ions were collected within a 150 µm diameter spot for imaging. Within this image field a lateral resolution of ~1 µm was realized.

RESULTS AND DISCUSSION

Effect of Cu on Passive Film Growth

Figure 1 shows logarithmic current-time plots recorded in the passive region (0.2 V_{SCE}) for both N06059 and N06200 at 60°C. Except for minor differences at short times, the plots are effectively

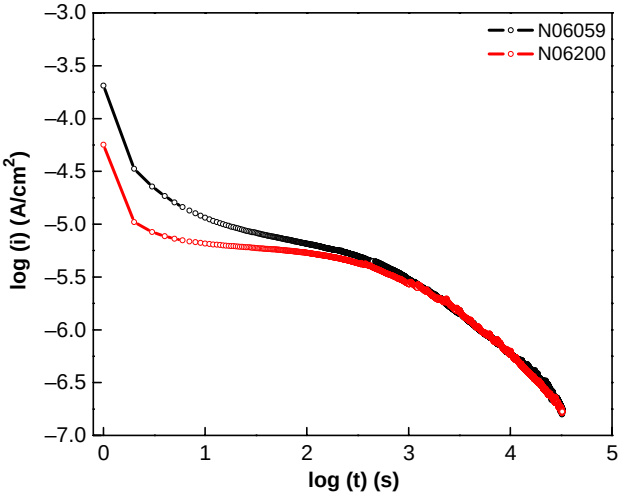

FIGURE 1. *Current-time plots recorded on N06059 and N06200 at 0.2 V_{SCE} in 1 M NaCl solution at 60°C.*

identical, indicating that the presence of Cu in N06200 exerted no observable effect on the kinetics of anodic film growth. This suggests the kinetics of film growth are dominantly controlled by the Cr and Mo contents, as observed previously for other Ni-Cr-Mo alloys.[38-39,41]

For Ni-Cr-Mo alloys,[38-39,41] the oxide film owes its passivity to its Cr/Mo content, which enforces the formation of an inner Cr(III) oxide barrier layer and an outer, dominantly hydroxide, Mo(VI) layer. With increasing temperature, the evolution in film properties was shown to involve two counterbalancing influences: an increase in overall film thickness, which would be expected to improve passivity, and a decrease in Cr/Mo content, which would be expected to degrade passivity.[39] This was shown to lead to anodic film growth and passive currents almost independent of temperature, up to at least 90°C, disguising the degradation of the film which eventually leads to its breakdown under crevice corrosion conditions. Figure 2 shows the anodic film growth on N06200 is similar and almost independent of pH. The shallow dependence on time for $t < 10^2$ s can be attributed to the change in composition and decrease in defect content of the cathodically reduced air-formed oxide remaining on the electrode surface after the cathodic pretreatment (60 min at –1.0 V).[39] For $t > 400$ s, the current density decreases logarithmically, as expected, and remains independent of pH. At long times ($>1.8 \times 10^4$ s [~5 h]), the current at pH = 1 becomes negative and dominated by proton reduction.

After film growth, the electrodes were analyzed by AR-XPS at take-off angles of 30° and 90°. Many examples of fitted XPS spectra have been published for Ni-Cr-Mo alloys[3-4,38-39] and only the conclusions drawn are shown here. The surface compositions determined from the survey spectra and the cation compositions of the films corrected for contributions from the metallic substrate (determined from high-resolution spectra) are shown in Figure 3. This figure shows that the O content of the surface decreases with a decrease in pH, indicating a decrease in film thickness, especially at pH = 1. This is confirmed by the analysis of high-resolution spectra which show an increase in the relative heights of the Ni2p and Cr2p peaks for the metals as opposed to oxides/hydroxides.

Also, as the pH decreases, the relative amounts of Mo and Cr in the oxide are enhanced while the Ni content decreases, especially within the inner regions of the film, as evidenced by the considerably larger pH-dependence observed for a take-off angle of 90° compared to one of 30°. The relatively high Mo/Cr and low Ni contents at the lowest pH can be attributed to an increase in anodic release of Ni from the inner layer as the pH decreases, resulting in a cleaner segregation of Cr(III) to the inner barrier layer and Mo(VI) to the outer surface, consistent with the results of Lloyd, et al.[3] A Cu2p signal is observed, indicating its enrichment in the surface but the amount appears insensitive to changes in pH. Whether or not Cu is present as Cu(I) or Cu cannot be determined as these oxidation states have similar binding energies.[33,38]

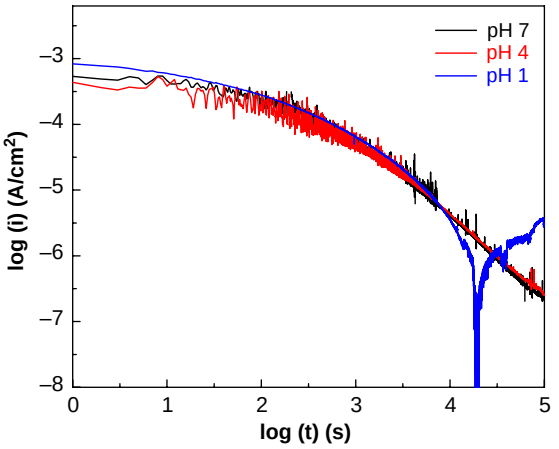

FIGURE 2. *Current-time plots recorded on N06200 at 0 V for three pH values.*

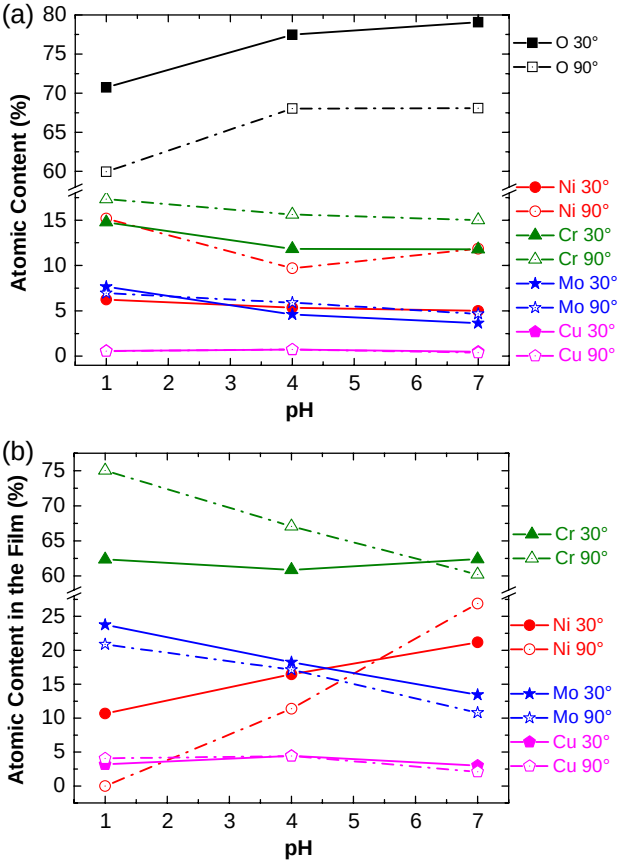

FIGURE 3. *(a) Surface composition of N06200 determined from survey spectra measured at take-off angles of 30° and 90° after anodic oxidation at 0 V (22°C, 44 h), and (b) film cation compositions. Corrected for contributions from the metallic components, determined from high-resolution spectra.*

Figure 4 shows the TOF-SIMS cross-sectional images reconstructed from the sputtering profiles recorded on the potentiostatically oxidized electrodes after the experiments at the three pH values. These images confirm the conclusions from the XPS experiments that the segregation of Cr (as Cr[III]) to the inner barrier layer and Mo (dominantly as Mo[VI]) to the outer layer is promoted as the pH decreases. This can be best appreciated by consideration of the CrO_3^-/MoO_3^- ion ratio (Figure 5). The slight decrease in this ratio as the pH decreases confirms a relative loss of Cr from the film as the pH decreases.

As with temperature,[39] the independence of film growth current on pH can be attributed to counterbalancing influences. The release of Ni(II) to the solution as the pH decreases leads to a more rapid development of the passive film bilayer, which would be expected to improve passivity. However, the accompanying thinning of the film predominantly resulting from the dissolution of the outer hydroxide accompanied by an overall loss of Cr would be expected to degrade passivity.

The cross-sectional images (Figure 4) also show an accumulation of Cu at the outer surface of the oxide.

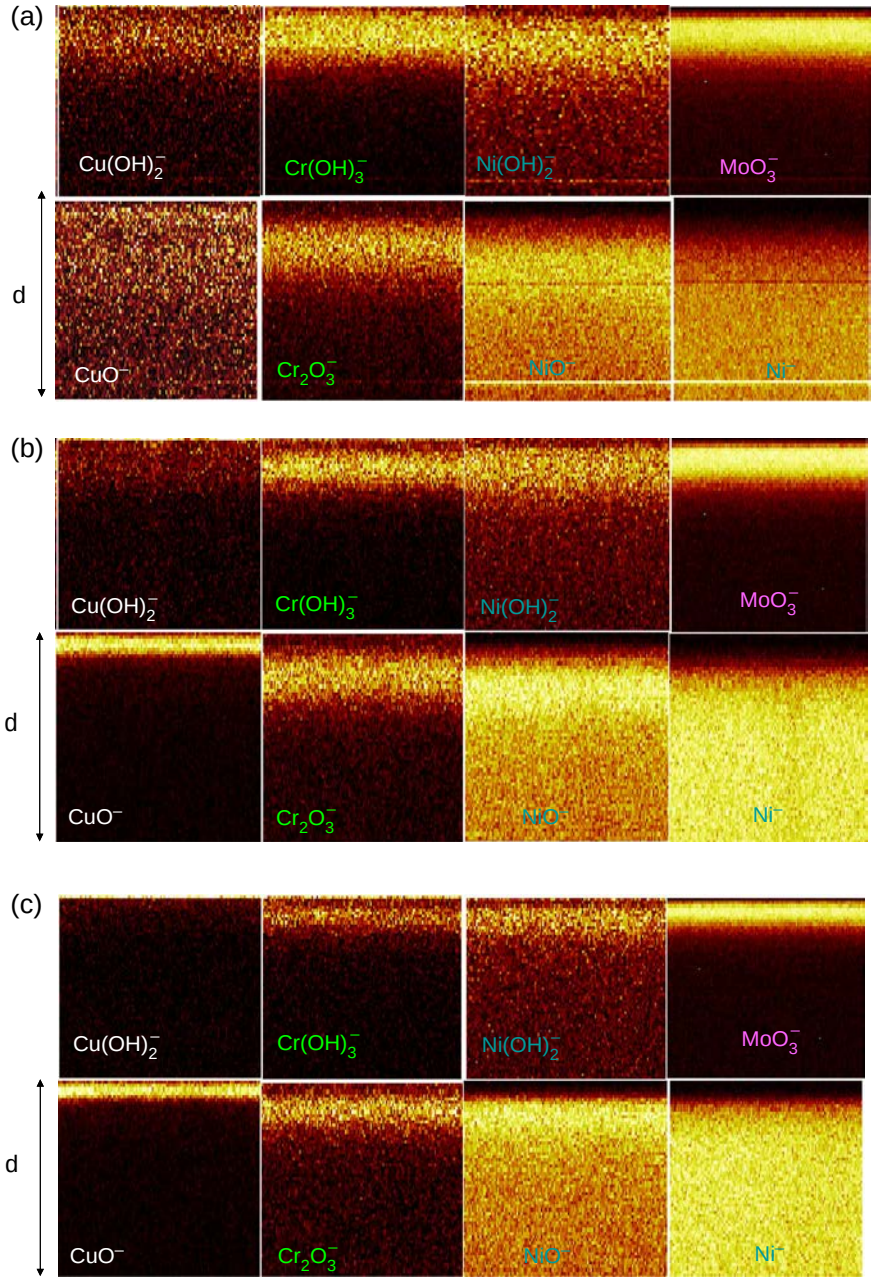

FIGURE 4. *TOF-SIMS cross-sectional images reconstructed from sputtering profiles for N06200 after anodic oxidations (Figure 2) at (a) pH 7, (b) pH 4, and (c) pH 1.*

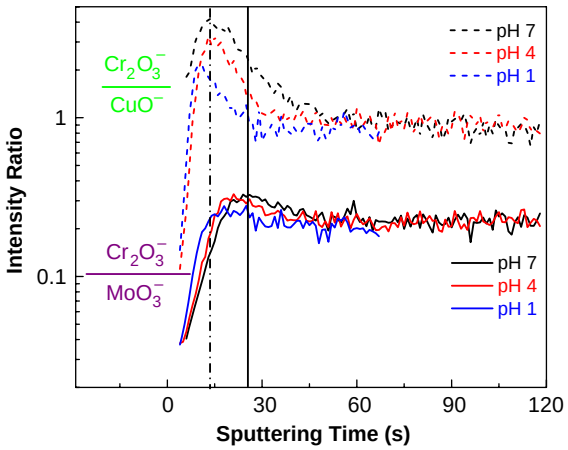

FIGURE 5. *$Cr_2O_3^-/MoO_3^-$ (solid lines) and Cr_2O_3/CuO^- (dotted lines) intensity ratios from TOF-SIMS sputtering profiles recorded on N06200 after anodic oxidations (Figure 2).*

This tendency to accumulate at the oxide/solution interface is more sharply concentrated at the two lower pH values, indicating that it accompanies the segregation of Cr(III) to the inner boundary layer and Mo(VI) to the outer oxide surface. This influence can be more readily appreciated from the Cr_2O_3/CuO^- ion ratio (Figure 5), which shows that the Cu content of the film not only becomes more concentrated at the outer surface, as clearly shown in the images, but also more concentrated in the inner layer compared to the Cr content (indicated by the decrease in the ratio with pH), despite the clearer presence of an inner Cr(III) barrier layer at lower pH.

Determination of Characteristic Potentials

Using the MCA arrangement, E_b and $E_{R,CREV}$ values were obtained by applying the PD-GS-PD technique, as has been done previously with a wide range of Ni-Cr-Mo alloys.[9] The potentiodynamic scans recorded in the first stage of these measurements are shown in Figure 6. While very similar, the currents in the passive region are slightly larger and more temperature dependent for the Cu-free N06059 than for the Cu-containing N06200, suggesting an ennoblement of the latter by the accumulation of Cu at the outer surface of the oxide film as the passive region is traversed. The behavior observed during the potentiodynamic and galvanostatic steps were only marginally different. For both alloys, stable crevice corrosion conditions were established for T ≥ 60°C and the values of E_b and $E_{R,CREV}$ were very similar (Figure 7). Although both alloys initiate crevice corrosion for T ≥ ~60°C (Figure 7), the time required for the establishment of stable crevice propagation was generally slightly lower for N06059 (e.g., ~5 h at 60°C) than for N06200 (e.g., ~9 h at 60°C), indicating that the presence of the surface Cu delayed the initiation of crevice propagation.

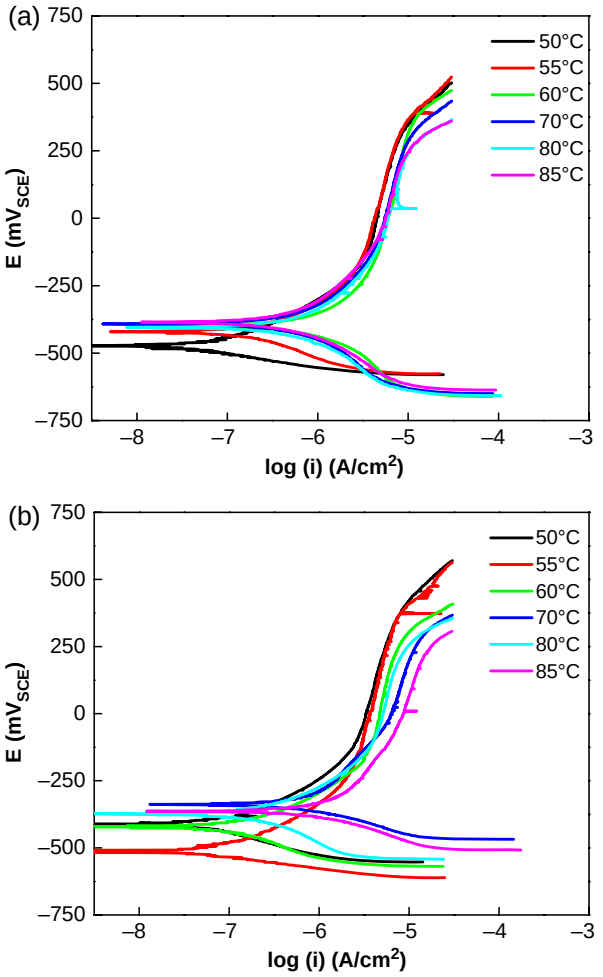

FIGURE 6. *Potentiodynamic polarization scans recorded on (a) N06200 and (b) N06059 in 1 M NaCl solution at various temperatures using the MCA arrangement.*

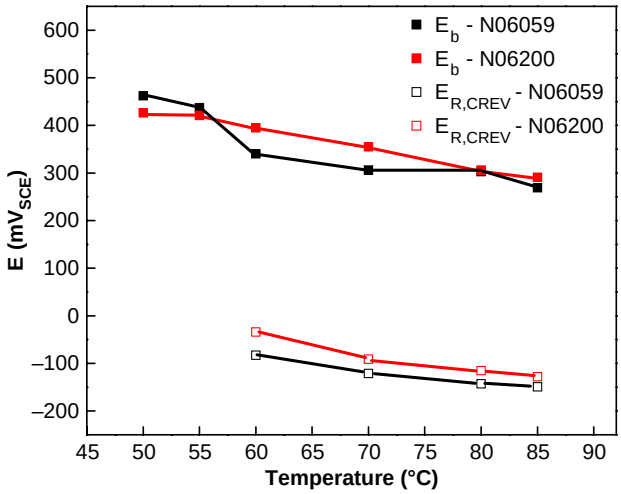

FIGURE 7. *Crevice breakdown (E_b) and repassivation ($E_{R,CREV}$) potentials as a function of temperature for N06059 and N06200 in 1 M NaCl solution.*

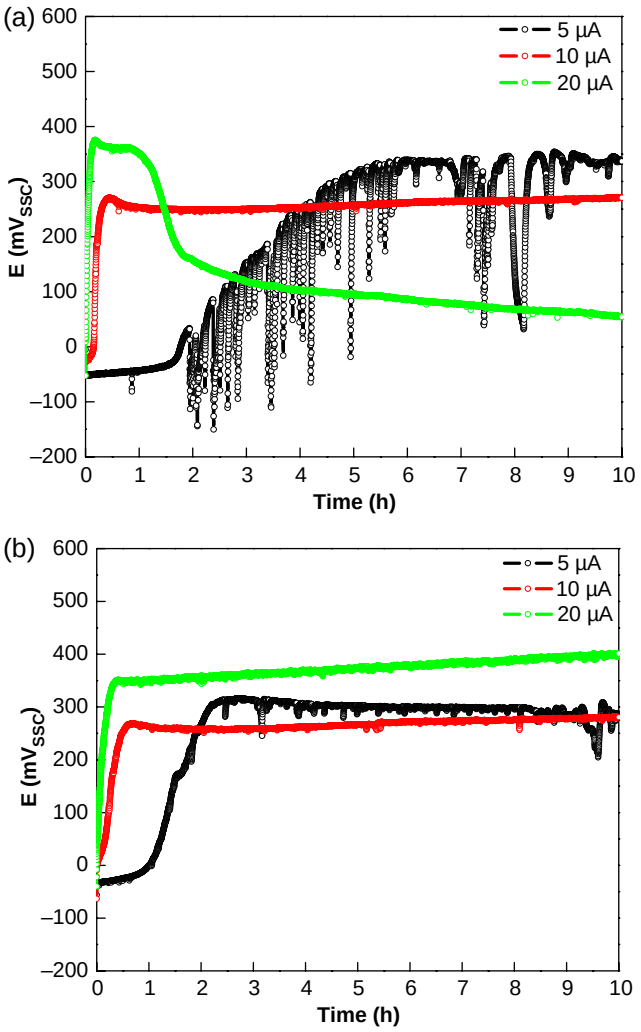

FIGURE 8. *Potential-time curves recorded at applied currents of 5 μA, 10 μA, and 20 μA on (a) N06059 and (b) N06200 in 1.0 M NaCl solution at 105°C using the SCA arrangement.*

Initiation of Stable Propagation

The dynamic conditions, large current (30 μA), and multiple crevices used in the PD-GS-PD experiment make it difficult to quantify the influence of Cu segregation during passive film formation on its influence on crevice initiation. In the SCA experiment, the evolution in film properties is driven by the applied current. At the constant temperature used in these experiments, the applied current enforces both the formation of the bilayer passive film and the formation of the Cu outer layer, and allows the crevice initiation process, when it occurs, to be followed.

Figures 8(a) and (b) show the potential-time curves recorded at an applied current of 5 μA, 10 μA, and 20 μA for N06059 and N06200 alloys. For 5 μA, the potential rises to ≥300 mV for both of the alloys. Although only the first 10 h are shown, the potential in both cases continued to rise slowly for both alloys, confirming that crevice corrosion did not initiate on either alloy over the duration of the experiment. The potential at the zero point in these plots is that established during the 1 h open circuit period prior to applying the current. The transients observed on N06059 indicate many unsuccessful attempts to initiate active crevice conditions (Figure 8[a]). These metastable events have the standard form of a rapid decrease followed by an exponential recovery expected for film breakdown-repair processes. The long duration (up to ~10 min) of these events suggests the initial loss of passivity requires a significant film regrowth to re-establish passivity. If the applied current is increased to 10 μA, the initial rise in potential is considerably more rapid and no significant metastable events are observed. At this higher applied current, any tendency toward film breakdown as the passive region is traversed (~−100 mV to ~250 mV) is quickly repaired, allowing the potential to increase more rapidly. By contrast, the absence of metastable transients on N06200 indicates a clear suppression of film breakdown events that can be attributed to the surface accumulation of Cu (Figure 8[b]). As transients events are almost eliminated and not just reduced in amplitude, the influence of Cu appears to be mainly the maintenance of passivity rather than its ennoblement of active breakdown sites.

This can be attributed to the segregation of Cu to the oxide film surface as acidic conditions develop within the crevice as a result of metal oxide dissolution and dissolved cation hydrolysis. A possible mechanism for the prevention of metastable events is that this segregation of Cu ennobles the surface, thereby preventing the breakdown event. However, when such events do occur, repassivation occurs rapidly, suggesting an ennoblement of the active metal surface may be involved.

The inability of either alloy to initiate a crevice at an applied current of only 5 μA is consistent with previous observations with Alloy 22 (Ni-22Cr-13Mo-3W, UNS N06022),[42] as are the observation of metastable events, adding credibility to the proposal that Cu eliminates these breakdown events. Although not shown, in the plots at an applied current of 10 μA, N06059 eventually succumbed to active crevice corrosion after ~38 h, while N06200 did not over the full 48 h of the experiment. If the applied current was further increased to 20 μA, both initiated crevice corrosion, N06059 after ~2 h and N06200 after ~15 h, confirming the ability of Cu to inhibit initiation.

This influence of Cu on metastable behavior is similar to that observed by Kim and Buchheit for Cu additions to Al.[30] As their measurements were conducted potentiostatically and involved the measurement of current transients on open surfaces, as opposed to these which measure potential transients on occluded surfaces, a direct comparison is not possible. However, both sets of experiments reflect the influence of Cu on localized passivity breakdown and

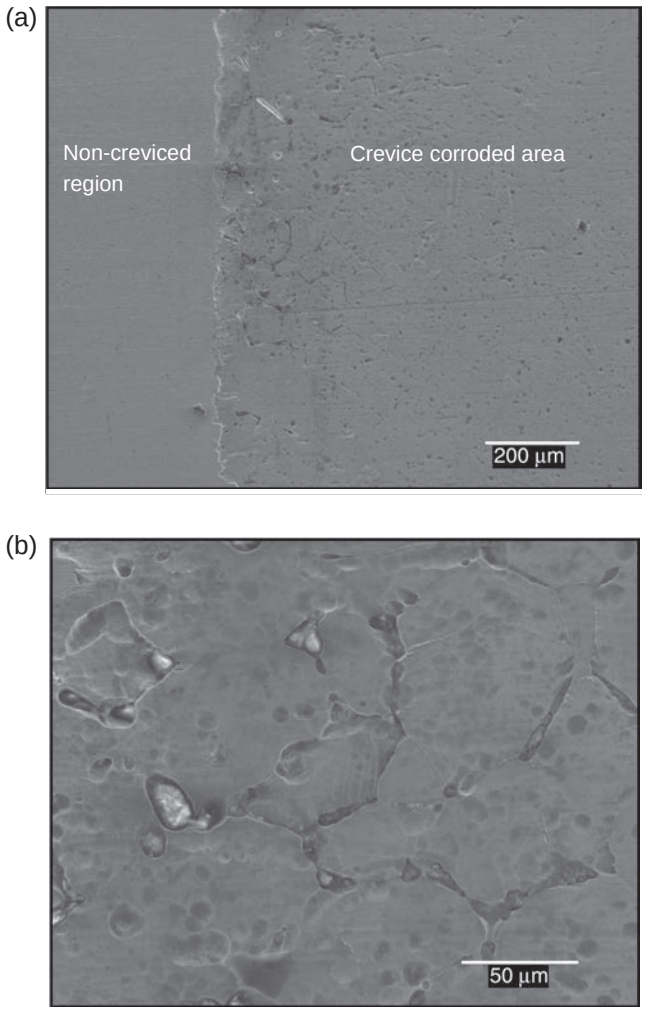

FIGURE 9. *SEM images of the N06200 SCA (48 h at 20 µA) showing (a) the non-creviced and crevice areas, and (b) a magnified view of the crevice corroded area just inside the crevice mouth.*

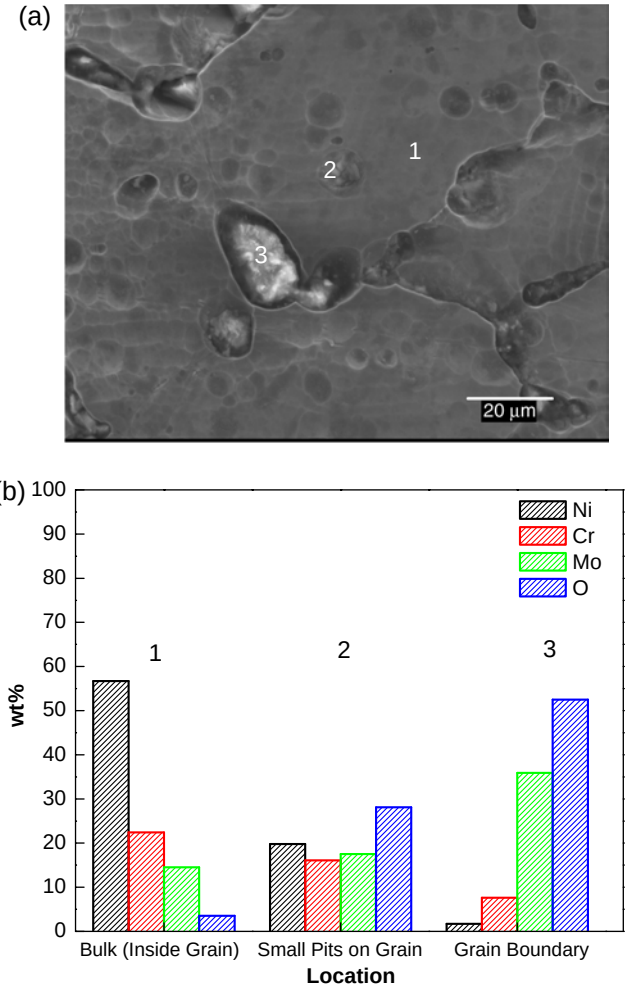

FIGURE 10. *(a) SEM image of a location within the crevice corroded region on N06200 (48 h at 20 µA), and (b) EDX spot analyses of the locations numbered in (a).*

temporary propagation of active sites. In both cases, Cu suppresses both the number of local site breakdowns and the amount of damage (alloy dissolution) occurring before passivity is re-established. These results indicate that the avoidance of local breakdown sites can be attributed to the segregation of Cu to the oxide/solution interface.

Characterization of Crevice Corroded Areas

Scanning Electron Microscopy and Energy-Dispersive X-Ray Spectroscopy Analyses — Figure 9 shows the crevice corroded area on N06200 after the experiment at an applied current of 20 µA using the single crevice assembly. Figure 9(a) shows that corrosion damage is predominantly located close to the crevice mouth with deep pits and channels on the grain boundaries and shallower pits on the surface of the grains. That some grain boundaries are deeply corroded while others are not is consistent with previous observations on Ni-Cr-Mo Alloys which showed that corrosion damage accumulated predominantly on random as opposed to Σ3 grain boundaries.[43]

EDX spot analyses were performed at different locations, as indicated by the numbers in the SEM image in Figure 10(a). For an uncorroded location on the surface of a grain (1), the elemental composition was representative of the bulk alloy, the small O signal confirming the presence of only a thin oxide (Figure 10[b]). Within a small pit on the surface of a grain (2 in Figure 10[a]), there is a clear loss of Ni and Cr and a slight enrichment of Mo with the enhanced O signal confirming Mo accumulates as an oxide. This is confirmed by the strongly enhanced O signal (Figure 10[b]). Analysis of the visible precipitate in the deeply corroded grain boundary (3) confirms the accumulation of Mo as oxide as corrosion progresses. These results are consistent with those observed previously on C-22† (UNS N06022), when Raman spectroscopy demonstrated the Mo was in the form of molybdates,[14] and with recent results recorded on the

alloys 625† (UNS N06625), N06022, and HYBRID-BC1† (UNS N10362) for which it was shown that the rate and extent of molybdate formation were the key factors limiting the depth of crevice penetration on these alloys.[44] A more general elemental mapping confirms that this behavior is observed uniformly across the crevice corroded area of the surface. These results confirm that crevice corrosion propagates on N06200 in a similar manner to that generally observed on Ni-Cr-Mo alloys.

Dynamic-Secondary Ion Mass Spectroscopy Analyses — The absence of any signal for Cu in the EDX analyses described earlier preempts any attempt to determine whether this element exerts any significant effect on the propagation process. Dynamic-SIMS, a more highly surface sensitive technique, can be used to detect elements present in only small amounts, although it provides no quantitative information.

The circle in the optical micrograph of the crevice corroded surface of N06200 (Figure 11[a]) indicates the locations at which the dynamic-SIMS experiment was performed (Figures 11[b] through [e]) for various sputtering times. After only a short period of sputtering (Figure 11[b]), a strong signal for Cu was observed in the deeply corroded grain boundaries and within the small pits on the grain surface. With increased sputtering time, the Cu signal remains, eventually disappearing on the grain surface as the deposit within the

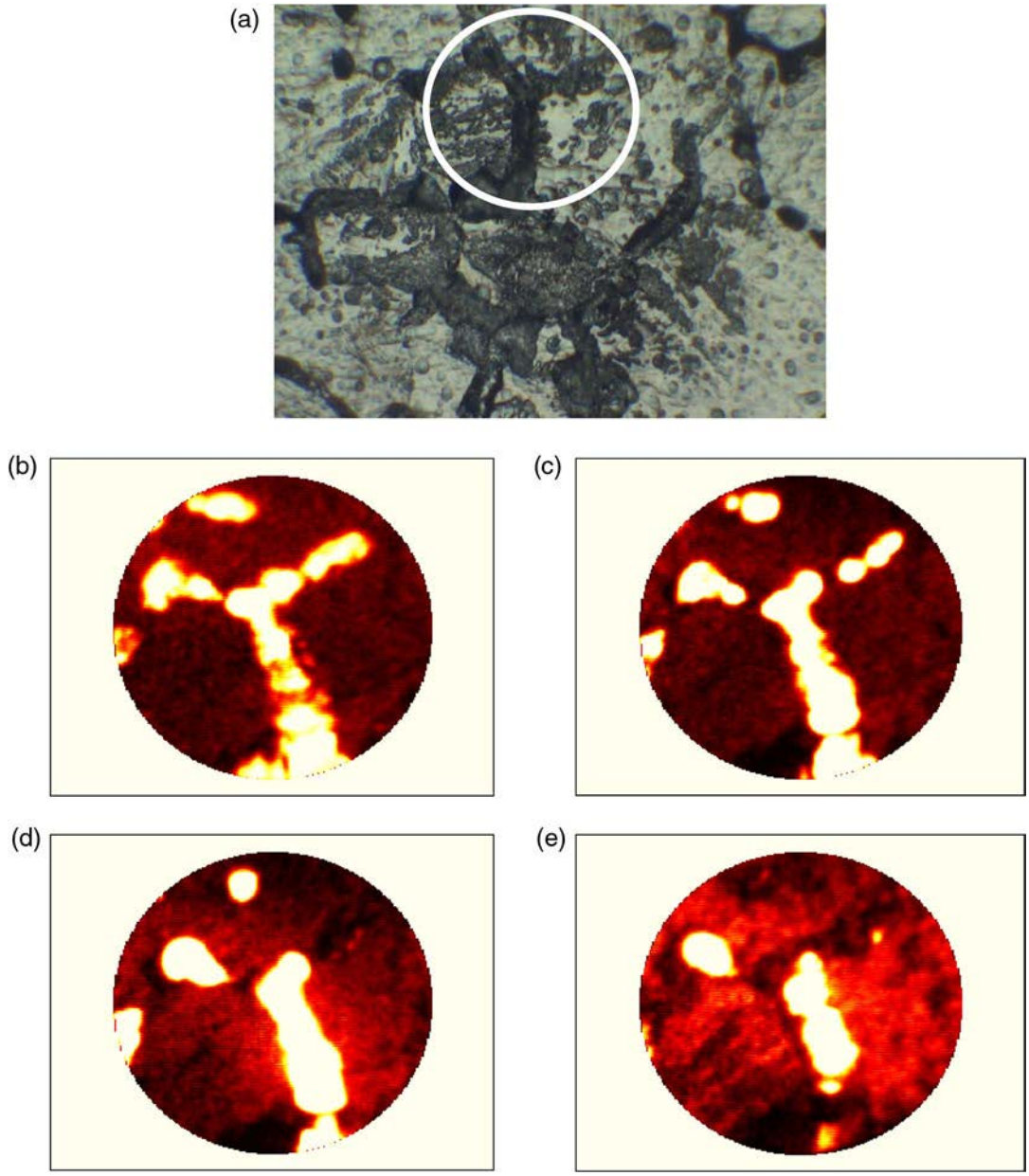

FIGURE 11. *(a) Optical micrograph showing a crevice corroded location on N06200 (48 h at 20 μA). (b) through (e) Dynamic-SIMS images of the area circled in (a) for Cu after different sputtering times: (b) 1 min, (c) 3 min, (d) 5 min, and (e) 15 min.*

small pit is removed by the sputtering. Because these corroded locations are those at which molybdates are deposited (as shown by the EDX analyses), these results demonstrate that the Cu is segregated to the outer surface of corroded locations. The persistence of the Cu signal with sputtering time shows that Cu is not just present as a thin surface layer but dispersed throughout the molybdate present at these locations. It seems likely that Cu is present as Cu(I), the stable oxidation state in concentrated chloride solutions,[45] but this cannot be verified by this technique. Because other Ni-Cr-Mo alloys, including N06059, which do not contain Cu exhibit similar damage patterns with the accumulations of molybdates at corroded locations, there is no evidence that Cu segregation in this manner provides any additional protection against crevice propagation, as has been suggested for the pitting of stainless steel.[26-27]

SUMMARY AND CONCLUSIONS

❖ Anodically formed passive oxides on alloys N06200 and N06059 show no significant differences in the growth kinetics.
❖ AR-XPS and TOF-SIMS demonstrated that the copper segregated to the oxide/solution interface during anodic film growth and that this process was enhanced as the pH decreased as would occur in a crevice prior to initiation.
❖ PD-GS-PD experiments using an MCA arrangement yield a very similar protection temperature and only a marginal improvement in repassivation potential for N06200 compared to N06059.
❖ Crevice corrosion experiments conducted galvanostatically using SCA demonstrate that crevice initiation is retarded on the Cu-containing N06200 compared to the Cu-free N06059.
❖ EDX analysis of crevice corroded regions on N06200 confirm that Ni and Cr are depleted, and Mo oxide accumulates, in crevice corroded regions. Dynamic-SIMS shows an enrichment of Cu in these corroded locations, but cannot demonstrate whether its presence inhibits crevice corrosion on N06200.
❖ The present study clearly demonstrates a non-detrimental role of Cu to localized corrosion when added in small amount in Ni-Cr-Mo alloy.
❖ The primary influence of Cu in Ni-Cr-Mo alloys appears to be its ability to inhibit crevice initiation by stifling the metastable pitting events that can eventually lead to the establishment of actively propagating locations. A similar claim has been made for Cu-containing Al alloys.[31] Additionally, the results are consistent with observations made on SS and support the conclusion that the primary influence of Cu in these alloys is its ability to ennoble the metal surface under active conditions. However, confirmation of ennoblement remains to be demonstrated.

ACKNOWLEDGMENTS

This research was funded by the Canadian Natural Sciences and Engineering Research Council (NSERC). The authors acknowledge Dr. H.Y. Nie, Dr. M. Biesinger, and Mr. Gary Good from Surface Science Western (Canada) in providing assistance to investigate the surface characterization data and Dr. Paul Crook from Haynes International (U.S.) for technical discussions.

REFERENCES

1. P. Crook, N.S. Meck, J. Crum, R.B. Rebak, "Corrosion of Nickel and Nickel-Base Alloys," in *Corrosion: Materials*, eds. S.D. Cramer, B.S. Covino Jr., ASM Handbook vol. 13B (Materials Park, OH: ASM International, 2005), p. 228-251.
2. J.R. Hayes, J.J. Gray, A.W. Szmodis, C.A. Orme, *Corrosion* 62 (2006): p. 491-500.
3. A.C. Lloyd, J.J. Noel, S. McIntyre, D.W. Shoesmith, *Electrochim. Acta* 49 (2004): p. 3015-3027.
4. A.C. Lloyd, D.W. Shoesmith, N.S. McIntyre, J.J. Noel, *J. Electrochem. Soc.* 150 (2003): p. B120-B130.
5. A.C. Lloyd, J.J. Noel, N.S. McIntyre, D.W. Shoesmith, *JOM* 57 (2005): p. 31-35.
6. R.S. Lillard, M.P. Jurinski, J.R. Scully, *Corrosion* 50 (1994): p. 251-265.
7. M.A. Rodriguez, *Corros. Rev.* 30 (2012): p. 19-32.
8. A.K. Mishra, G.S. Frankel, *Corrosion* 64 (2008): p. 836-844.
9. A.K. Mishra, D.W. Shoesmith, *Corrosion* 70 (2014): p. 721-730.
10. K.J. Evans, A. Yilmaz, S.D. Day, L.L. Wong, J.C. Estill, R.B. Rebak, *JOM* 57 (2005): p. 56-61.
11. M.A. Rodriguez, R.M. Carranza, R.B. Rebak, *Corrosion* 66 (2010): p. 1-14.
12. N.S. Zadorozne, C.M. Giordano, M.A. Rodriguez, R.M. Carranza, R. B. Rebak, *Electrochim. Acta* 76 (2012): p. 94-101.
13. X. Shan, J.H. Payer, *J. Electrochem. Soc.* 156 (2009): p. C313-321.
14. P. Jakupi, F. Wang, J.J. Noel, D.W. Shoesmith, *Corros. Sci.* 53 (2011): p. 1670-1679.
15. S.S. Haudet, M.A. Rodriguez, R.M. Carranza, "Effect of Alloy Composition on the Localized Corrosion of Nickel Alloys," in *Scientific Basis for Nuclear Waste Management XXXV*, eds. R.M. Carranza, G.S. Duffo, R.B. Rebak, MRS Symposium Proceedings, vol. 1475 (New York, NY: Cambridge University Press, 2012), p. 489.
16. T. Sourisseau, E. Chauveau, B. Baroux, *Corros. Sci.* 47 (2005): p. 1097-1117.
17. H.T. Lin, W.T. Tsai, J.T. Lee, C.S. Huang, *Corros. Sci.* 33 (1992): p. 691-697.
18. Y. Jiangnan, W. Lichang, S. Wenhao, *Corros. Sci.* 33 (1992): p. 851-859.
19. M. Seo, G. Hultquist, C. Leygraf, N. Sato, *Corros. Sci.* 26 (1986): p. 949-960.
20. G. Hultquist, M. Seo, T. Leitner, C. Leygraf, N. Sato, *Corros. Sci.* 27 (1987): p. 937-946.
21. D. Itzhak, P. Peled, *Corros. Sci.* 26 (1986): p. 49-54.
22. P. Peled, D. Itzhak, *Corros. Sci.* 32 (1991): p. 83-90.
23. J. Banas, A. Mazurkiewicz, *Mater. Sci. Eng. A* 277 (2000): p. 183-191.
24. A. Pardo, M.C. Merino, M. Carboneras, A.E. Coy, R. Arrabal, *Corros. Sci.* 49 (2007): p. 510-525.
25. T. Ujiro, S. Satoh, R.W. Staehle, W.H. Smyrl, *Corros. Sci.* 43 (2001): p. 2185-2200.
26. L.F. Garfias-Mesias, J.M. Sykes, *Corrosion* 54 (1998): p. 40-47.
27. L. Freire, X.R. Novoa, G. Pena, V. Vivier, *Corros. Sci.* 50 (2008): p. 3205-3212.
28. A.A. Hermas, K. Ogura, S. Takagi, T. Adachi, *Corrosion* 51 (1995): p. 3-10.
29. I.L. Muller, J.R. Galvale, *Corros. Sci.* 177 (1977): p. 179-193.
30. Y. Kim, R.G. Buchheit, *Electrochim. Acta* 52 (2007): p. 2437-2446.
31. Y. Kim, R.G. Buchheit, P.G. Kotula, *Electrochim. Acta* 55 (2010): p. 7367-7375.
32. M. Pourbaix, *Atlas of Electrochemical Equilibria in Aqueous Solutions* (Houston, TX: NACE International, 1974), p. 387.
33. M.C. Biesinger, L.W.M. Lau, A.R. Gerson, R.S. Smart, *Appl. Surf. Sci.* 257 (2010): p. 887-898.

34. N. Sridhar, *MP* 27 (1988): p. 40-46.
35. P. Crook, "Development of a New Ni-Cr-Mo Alloy," CORROSION 1996, paper no. 412 (Houston, TX: NACE, 1996).
36. P. Crook, M.L. Caruso, D.A. Kingseed, *MP* 36 (1997): p. 49-52.
37. L. VanGansbeke, L. Paul, D. Kingseed, "Experience with the New Ni-Cr-Mo Alloy UNS N06200 in Flue Gas Desulfurization (FGD) Systems," CORROSION 2000, paper no. 582 (Houston, TX: NACE, 2000).
38. X. Zhang, D. Zagidulin, D.W. Shoesmith, *Electrochim. Acta* 89 (2013): p. 814-822.
39. X. Zhang, D.W. Shoesmith, *Corros. Sci.* 76 (2013): p. 424-431.
40. X. He, J.J. Noel, D.W. Shoesmith, *J. Electrochem. Soc.* 149 (2002): p. B440-B4449.
41. D. Zagidulin, X. Zhang, J. Zhou, J.J. Noel, D.W. Shoesmith, *Surf. Interface Anal.* 45 (2013): p. 1014-1019.
42. P. Jakupi, J.J. Noel, D.W. Shoesmith, *Corros. Sci.* 53 (2011): p. 3122-3130.
43. P. Jakupi, J.J. Noel, D.W. Shoesmith, *Electrochem. Solid-State Letters* 13 (2010): p. C1-C3.
44. N. Ebrahimi, P. Jakupi, J.J. Noel, D.W. Shoesmith, *Corrosion* 71, 12 (2015): p. 1441-1451.
45. G. Kear, B.D. Barker, F.C. Walsh, *Corros. Sci.* 46 (2004): p. 109-135.